Phys Chem Minerals (2010) 37:227–236
DOI 10.1007/s00269-009-0327-x

ORIGINAL PAPER

Stability at high pressure, elastic behavior and pressure-induced structural evolution of "Al_5BO_9", a mullite-type ceramic material

G. Diego Gatta · Nicola Rotiroti · Martin Fisch · Thomas Armbruster

Received: 22 May 2009 / Accepted: 29 August 2009 / Published online: 22 September 2009

Abstract Elastic behavior and pressure-induced structural evolution of synthetic boron-mullite "Al_5BO_9" (a = 5.678(2) Å, b = 15.015(4) Å and c = 7.700(3) Å, space group $Cmc2_1$, $Z = 4$) were investigated up to 7.4 GPa by in situ single-crystal X-ray diffraction with a diamond anvil cell under hydrostatic conditions. No phase transition or anomalous compressional behavior occurred within the investigated P range. Fitting the P–V data with a truncated second-order (in energy) Birch-Murnaghan Equation-of-State (BM-EoS), using the data weighted by the uncertainties in P and V, we obtained: $V_0 = 656.4(3)$ Å^3 and $K_{T0} = 165(7)$ GPa ($\beta_{V0} = 0.0061(3)$ GPa^{-1}). The evolution of the Eulerian finite strain versus normalized stress (f_E–F_E plot) leads to an almost horizontal trend, showing that a truncated second-order BM-EoS is appropriate to describe the elastic behavior of "Al_5BO_9" within the investigated P range. The weighted linear regression through the data points gives: $F_E(0) = 159(11)$ GPa. Axial compressibility coefficients yielded: $\beta_a = 1.4(2) \times 10^{-3}$ GPa^{-1}, $\beta_b = 3.4(4) \times 10^{-3}$ GPa^{-1}, and $\beta_c = 1.7(3) \times 10^{-3}$ GPa^{-1} (β_a:β_b:β_c = 1:2.43:1.21). The highest compressibilities observed in this study within (100) can be ascribed to the presence of voids represented by five-membered rings of polyhedra: Al1–Al3–Al4–Al1–Al3, which allow accommodating the effect of pressure by polyhedral tilting. Polyhedral tilting around the voids also explains the higher compressibility along [010] than along [001]. The stiffer crystallographic direction observed here might be controlled by the infinite chains of edge-sharing octahedra running along [100], which act as "pillars", making the structure less compressible along the a-axis than along the b- and c-axis. Along [100], compression can only be accommodated by deformation of the edge-sharing octahedra (and/or by compression of the Al–O bond lengths), as no polyhedral tilting can occur. In addition, a comparative elastic analysis among the mullite-type materials is carried out.

Keywords Al_5BO_9 · Mullite · Sillimanite · Al_2O_3–B_2O_3–SiO_2 · Compressibility · Elastic behavior · P-induced structure evolution

Introduction

Compounds with chemical composition belonging to the ternary system Al_2O_3–B_2O_3–SiO_2 are a class of ceramic materials investigated in particular for industrial applications. Their high-temperature stability, low-thermal expansion coupled with high-creep resistance, low-electric conductivity, high-chemical stability and low density are leading to an increasing number of outstanding applications of such materials: as construction and engineering ceramics, refractory linings due to their high resistance to corrosion, optically translucent ceramics for high-temperature furnace windows, fire-protecting linings in nuclear

Electronic supplementary material The online version of this article (doi:10.1007/s00269-009-0327-x) contains supplementary material, which is available to authorized users.

G. D. Gatta (✉) · N. Rotiroti
Dipartimento di Scienze della Terra,
Università degli Studi di Milano, Via Botticelli 23,
20133 Milan, Italy
e-mail: diego.gatta@unimi.it

G. D. Gatta · N. Rotiroti
CNR-Istituto per la Dinamica dei Processi Ambientali,
Milan, Italy

M. Fisch · T. Armbruster
Institute of Geological Sciences, Mineralogical Crystallography,
University of Bern, Freiestrasse 3, 3012 Bern, Switzerland

plants due to the low density and the capability of absorbing neutrons, substrates for catalytic convertors, and electronic devices (Fischer and Schneider 2005, 2008; Li and Chang 2006; Peng et al. 2006; Tang et al. 2006; Zhang et al. 2006; Tao et al. 2007; Wei et al. 2007). Among those, mullite $[Al_2(Al_{2+2x}Si_{2-2x})O_{10-x}$ with $\sim 0.2 < x < \sim 0.9$ and $B_2O_3 = 0]$ (Saalfeld and Guse 1981; Angel et al. 1991; Schneider and Komarneni 2005) is doubtless of great importance. Several studies have been devoted to the stability fields, solubility and crystal chemistry of the compounds belonging to the ternary system Al_2O_3–B_2O_3–SiO_2 (Baumann and Moore 1942; Letort 1952; Dietzel and Scholze 1955; Scholze 1956; Gielisse and Foster 1962; Kim and Hummel 1962; Capponi et al. 1972; Reynaud 1977; Sokolova et al. 1978; Werding and Schreyer 1984, 1992, 1996; Rymon-Lipinski et al. 1985; Mazza et al. 1992; Peacor et al. 1999; Fischer and Schneider 2005, 2008; Buick et al. 2008; Fischer et al. 2008; Grew et al. 2008; Griesser et al. 2008). In their recent review paper on crystal chemistry of boroaluminosilicates with mullite-type structures, Fischer and Schneider (2008) described the structural relationship in the Al_2O_3–B_2O_3–SiO_2 compounds, showing that all boron-mullites can be derived from a hypothetical aristotype with topological symmetry *P*4/*mbm*, in which the main building block is represented by chains of edge-sharing MO_6-octahedra running along [001].

Thermo-elastic behavior and pressure (*P*) and temperature (*T*) structural evolution of aluminosilicates along the joint Al_2O_3–SiO_2 have been extensively investigated by Brillouin spectroscopy (Vaughan and Weidner 1978) and by in situ X-ray/neutron single-crystal/powder diffraction (Brace et al. 1969; Winter and Ghose 1979; Ralph et al. 1984; Schneider and Eberhard 1990; Comodi et al. 1997; Yang et al. 1997a, b; Brunauer et al. 2001; Friedrich et al. 2004; Burt et al. 2006; Gatta et al. 2006a, b; Schneider et al. 2008). The *P*/*T*-induced main deformation mechanisms were described on the basis of in situ H*P*/H*T* structure refinements. For $2Al_2O_3{\cdot}SiO_2$ mullite, a full description of the elastic properties [i.e. stiffness coefficients (c_{ij}), elastic compliances (s_{ij}), Young's moduli (E_{ij}), Poisson's ratios (v_{ij}), bulk modulus (*K*) and shear modulus (*G*)] was reported by Hildmann et al. (2001) by single-crystal resonant ultrasound spectroscopy (RUS); temperature derivatives of the elastic constants between −170 and 1,400°C were later derived by Schreuer et al. (2006) by single-crystal RUS. The elastic constants and their *T* derivatives of $2.5Al_2O_3{\cdot}SiO_2$ mullite have been reported by Kriven et al. (1999) and Palko et al. (2002) by Brillouin spectroscopy. In contrast, no elastic data are available for boroaluminates or boroaluminosilicates.

The aim of the present study was to investigate the elastic behavior and *P*-induced structural evolution of a boroaluminate by means of in situ single-crystal X-ray diffraction, with a diamond anvil cell (DAC), in order to elucidate the role of boron on the elastic features of mullite-type materials. We selected the "Al_5BO_9" compound for this first H*P* experiment.

Two slightly different compositions of the investigated compound are present in literature: Baumann and Moore (1942), Ihara et al. (1980) and Garsche et al. (1991) interpreted the material as $9Al_2O_3{\cdot}2B_2O_3$ ($Al_{4.91}B_{1.09}O_9$, $Z = 4$, commonly cited as $Al_{18}B_4O_{33}$), whereas Sokolova et al. (1978) concluded the compound to consist of $10Al_2O_3{\cdot}2B_2O_3$ (Al_5BO_9, $Z = 4$). In $Al_{18}B_4O_{33}$, 9% of aluminum tetrahedra are substituted by fourfold-coordinated boron. In Al_5BO_9, boron is only present on a threefold-coordinated site. In this study, test single-crystal X-ray refinements with boron constraint to the threefold-coordinated site were superior to refinements with excess boron according to $Al_{4.91}B_{1.09}O_9$. For this reason, the investigated compound is here referred to as "Al_5BO_9".

Sokolova et al. (1978) described the structure in space group $Cmc2_1$ ($a = 5.6673(7)$ Å, $b = 15.011(2)$ Å, $c = 7.693(1)$ Å), consisting of mullite-type octahedral chains (in this set running along [100]), linked by edge-sharing AlO_5 bipyramids alternating with AlO_4 tetrahedra and BO_3 triangular units (Fig. 1). In their classification of mullite-type materials, Fischer and Schneider (2008) assigned this compound to the "MUL-VIII.33, $Bb2_1m$: A_9B_2" group, together with $Al_{18}B_4O_{33}$, $Al_9BSi_2O_{19}$ (boromullite) and $Al_{16.6}Cr_{1.4}B_4O_{33}$. Due to the structural homologies with mullite, the authors considered the terms "boron-mullite" and "B-mullite" as appropriate for "Al_5BO_9". Garsche et al. (1991) showed that Cr^{3+} can replace Al^{3+} at the octahedral site in $Al_{18}B_4O_{33}$ up to about 10 wt.% Cr_2O_3. A further Al_5BO_9 structural model was reported by Mazza et al. (1992), with a pseudo-tetragonal unit cell ($a \sim b \sim 7.6$ Å and $c \sim 2.8$ Å) in space group *Pbam*. This compound is supposed to be metastable and transforms to equilibrium phase upon heating (Fischer and Schneider 2008).

Experimental methods

"Al_5BO_9" crystals were synthesized by slow cooling of a starting mixture in a flux consisting of 0.50 g K_2CO_3 and 1.56 g MoO_3 corresponding to $1K_2CO_3 + 3MoO_3 \rightarrow K_2Mo_3O_{10} + CO_2\uparrow$. The starting mixture was composed of Al_2O_3 and B_2O_3 mixed in a molar ratio of 9:2 (0.03 g B_2O_3 and 0.19 g Al_2O_3). All compounds were ground for 10 min in an agate mortar and placed in a lid-covered platinum crucible. The mixture was heated to 800°C at a gradient of 100°C/h and then further heated to 1,100°C at a rate of 50°C/h. After 2 h at 1,100°C, the melt was slowly cooled down to 600°C at 10°C/h.

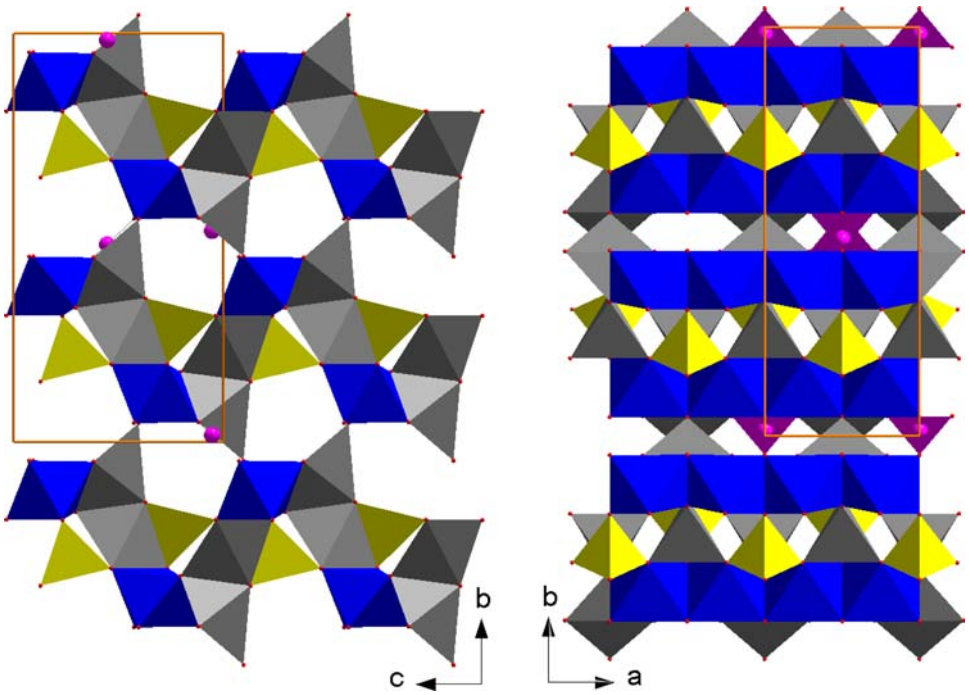

Fig. 1 The crystal structure of "Al_5BO_9" viewed down [100] (*left side*) and down [001] (*right side*) in $Cmc2_1$. Octahedra are represented in *blue*, distorted bipyramidal polyhedra in *gray*, tetrahedra in *yellow* and triangular BO_3 units in *purple* (*purple spheres* represent the B-sites). The edge-sharing octahedral chains running along [100] are well evident (*right side*), as well as the distorted five-membered rings of polyhedra forming the voids (*left side*)

Separation of the whitish, half-transparent crystals from yellowish flux was done by soaking the melt in hot water. Yield was about 0.1 g of radially grown aggregates of needle-like crystals with a maximum size of about $0.2 \times 0.2 \times 0.8$ mm^3.

One platy crystal ($180 \times 140 \times 60$ μm^3), free of defects or twinning under the transmitting polarized light microscope, was selected for X-ray diffraction experiments. Diffraction data were first collected at room conditions with an Oxford Diffraction-Xcalibur diffractometer equipped with CCD, using graphite monochromatized Mo$K\alpha$ radiation, operated at 50 kV and 40 mA. A combination of ω/φ scans was used in order to maximize the reciprocal space coverage and redundancy, with a scan width of 0.4° and an exposure time of 30 s/frame (Table 1). The distance between the crystal and the detector was 80 mm. 7,265 Bragg reflections were collected in the range $2° < 2\theta < 70°$, of which 1,302 were unique and 926 with $F_o > 4\sigma(F_o)$ (Table 1). The diffraction pattern was fully indexed with an orthorhombic lattice with $a = 5.678(2)$ Å, $b = 15.015(4)$ Å and $c = 7.700(3)$ Å, in agreement with the experimental findings of Sokolova et al. (1978) for "Al_5BO_9". Integrated intensities were then corrected for Lorentz polarization (Lp) and for absorption effects (by Gaussian integration based upon the shape and dimensions of the crystal), using the CrysAlis package (2005). After corrections, the discrepancy factor among symmetry-related reflections (Laue class *mmm*) was $R_{int} = 0.074$ (Table 1) and reflection conditions were consistent with space group $Cmc2_1$, as reported by Sokolova et al. (1978). The anisotropic structural refinement was then performed using the SHELX-97 software (Sheldrick 1997), starting from atomic coordinates of Sokolova et al. (1978). The refined Flack parameter (Sheldrick 1997) was 0 within $1\sigma(x)$. Neutral atomic scattering factors of B, Al and O from the International Tables for Crystallography (Wilson and Prince 1999) were used. No peak larger than $+0.82/-0.61$ e^-/Å^3 was present in the final difference-Fourier synthesis and the variance–covariance matrix showed no significant correlation between refined parameters. Further details pertaining to the structural refinement at ambient conditions are reported in Tables 1 and 2.

An ETH-type DAC (Miletich et al. 2000) was used to perform the in situ high-pressure experiment. 250-μm-thick T301 steel foil was used as gasket, which was pre-indented to a thickness of about 110 μm before drilling a 300 μm hole by spark erosion. The crystal of "Al_5BO_9" already measured at ambient conditions was placed into the gasket hole together with a single crystal of quartz for pressure calibration (Angel et al. 1997). A methanol:ethanol mixture (4:1) was used as hydrostatic pressure-transmitting medium (Angel et al. 2007). Intensity data collections at 0.0001 GPa (crystal in DAC without any pressure medium, P_0), 0.15(5) (P_1), 0.91(5) (P_2), 1.99(6) (P_3), 3.32(6) (P_4), 4.78(6) (P_5), 5.83(5) (P_6), 5.99(5) (P_7) and 6.45(6) (P_8) GPa (Table 1) were performed adopting the same experimental set-up and data collection protocol used with the crystal in air (Table 1). At any given pressure, integrated intensity data were corrected for Lp and absorption

Table 1 Details pertaining to the data collections and refinements of "Al_5BO_9" at different pressures

	P (GPa)									
	0.0001	0.0001[a] (P_0)	0.15(5) (P_1)	0.91(4) (P_2)	1.99(6) (P_3)	3.32(6) (P_4)	4.78(6) (P_5)	5.83(5) (P_6)	5.99(5) (P_7)	6.45(6) (P_8)
Diffractometer	Xcalibur CCD	Xcalibur CCD	Xcalibur CCD	Xcalibur CCD	Xcalibur CCD	Xcalibur CCD	Xcalibur CCD	Xcalibur CCD	Xcalibur CCD	Xcalibur CCD
X-ray radiation	Mo*K*α	Mo*K*α	Mo*K*α	Mo*K*α	Mo*K*α	Mo*K*α	Mo*K*α	Mo*K*α	Mo*K*α	Mo*K*α
Scan type	ω/φ	ω/φ	ω/φ	ω/φ	ω/φ	ω/φ	ω/φ	ω/φ	ω/φ	ω/φ
Scan width (°/frame)	0.4	0.4	0.4	0.4	0.4	0.4	0.4	0.4	0.4	0.4
Exposure (s/frame)	30	30	30	30	30	30	30	30	30	30
Temperature (K)	298	298	298	298	298	298	298	298	298	298
Space group	$Cmc2_1$	$Cmc2_1$	$Cmc2_1$	$Cmc2_1$	$Cmc2_1$	$Cmc2_1$	$Cmc2_1$	$Cmc2_1$	$Cmc2_1$	$Cmc2_1$
Cell dim. (Å)										
a	5.678(2)	5.680(3)	5.677(3)	5.668(4)	5.662(4)	5.655(4)	5.648(4)	5.639(4)	5.641(2)	5.639(4)
b	15.015(4)	15.02(60)	15.020 (50)	14.990(30)	14.940(30)	14.860(30)	14.790(20)	14.760(40)	14.760(30)	14.730(30)
c	7.700(3)	7.698(2)	7.694(4)	7.683(6)	7.669(6)	7.652(7)	7.644(7)	7.635(17)	7.626(5)	7.618(7)
Z	4	4	4	4	4	4	4	4	4	4
Maximum 2θ (°)	70.02	77.99	78.02	78.40	78.02	77.07	77.60	75.61	78.09	77.37
Measured reflections	7265	1672	1421	1570	1580	1659	1641	1613	1609	1279
Unique reflections	1302	411	503	603	585	600	555	538	534	463
Unique reflections with $F_o > 4\sigma(F_o)$	926	311	350	361	357	401	402	383	385	307
R_{int}	0.0739	0.1011	0.1007	0.1315	0.1163	0.1260	0.1131	0.1199	0.0952	0.1009
Number of l.s. parameters	82	31	30	30	30	30	30	30	30	30
R_1, $F_o > 4\sigma(F_o)$	0.0444	0.0753	0.0845	0.0866	0.0919	0.1098	0.1089	0.1020	0.1182	0.1187
wR_2	0.0821	0.1109	0.1181	0.1270	0.1268	0.1417	0.1305	0.1313	0.1437	0.1320
GooF	1.001	1.274	1.084	1.008	1.041	1.220	1.252	1.215	1.367	1.223

$R_{int} = \sum |F^2_{obs} - F^2_{obs}(mean)| / \sum (F^2_{obs})$; $R_1 = \sum (|F_{obs}| - |F_{calc}|) / \sum |F_{obs}|$; $wR_2 = \left(\sum (w(F^2_{obs} - F^2_{calc})^2) / \sum (w(F^2_{obs})^2) \right)^{0.5}$; $w = 1/(\sigma^2 (F^2_{obs}) + (0.02P)^2)$; $P = (\mathrm{Max}(F^2_{obs}, 0) + 2F^2_{calc})/3$

[a] With the crystal in the DAC without *P* medium

effects due to the crystal and the DAC using the ABSORB 5.2 computer program (Burnham 1966; Angel 2002). No violation of reflection conditions dictated by space group $Cmc2_1$ was observed within the investigated *P* range. The structure refinements were conducted using soft geometrical restraints aimed to restrain Al–O and B–O distances to those obtained at room pressure in air, with an estimated standard deviation of ±0.04 Å. This improved the stability of the H*P* refinements, as soft restrains act as if they were additional experimental observations (Sheldrick 1997; Gatta et al. 2006a, b, 2008). In order to reduce the number of refined variables, isotropic displacement parameters were refined by grouping all of the Al-sites and all of the O-sites. Refined atomic positions and displacement parameters are reported in Table 2. Bond distances and angles are listed in Table 3 (deposited as electronic supplementary file). At 7.4 GPa, the gasket hole collapsed and the "Al_5BO_9" crystal was incidentally broken. Unit-cell constants measured at ambient conditions after decompression using a small fragment of the "Al_5BO_9" crystal ($60 \times 40 \times 30$ μm^3) recovered from the gasket hole showed that *P*-induced structural changes up to 7.4 GPa are completely reversible.

Elastic behavior

The monotonic variation of "Al_5BO_9" unit-cell parameters with pressure is shown in Fig. 2. No evidence of phase transition or change in the compressional behavior were observed within the investigated pressure range. The elastic behavior of "Al_5BO_9" is described with a truncated second-order Birch-Murnaghan Equation-of-State (II-BM-EoS) (Birch 1947). This EoS is based upon the assumption

Table 2 Atomic coordinates and displacement parameters (Å^2) of "Al_5BO_9" at different pressures

Sites	P (GPa)	x	y	z	U_{iso}, U_{eq}
Al1	0.0001	0.2519(2)	0.11653(6)	0.3336(2)	0.0069(2)
8*b*	P_0^a	0.2513(4)	0.1155(8)	0.3337(4)	0.0072(4)
	P_1	0.2521(3)	0.1171(6)	0.3343(4)	0.0079(4)
	P_2	0.2521(4)	0.1167(4)	0.3304(5)	0.0082(4)
	P_3	0.2513(4)	0.1164(4)	0.3326(6)	0.0086(4)
	P_4	0.2528(5)	0.1174(4)	0.3325(5)	0.0090(5)
	P_5	0.2520(5)	0.1171(4)	0.3328(6)	0.0086(4)
	P_6	0.2518(5)	0.1171(4)	0.3333(6)	0.0081(4)
	P_7	0.2524(6)	0.1172(5)	0.3325(7)	0.0084(5)
	P_8	0.2517(7)	0.1160(6)	0.3326(7)	0.0077(5)
Al2	0.0001	0	0.25515(9)	0.5199(2)	0.0096(4)
4*a*	P_0^a	0	0.2590(8)	0.5208(5)	0.0072(4)
	P_1	0	0.2547(6)	0.5216(6)	0.0079(4)
	P_2	0	0.2552(5)	0.5216(6)	0.0082(4)
	P_3	0	0.2561(4)	0.5198(6)	0.0086(4)
	P_4	0	0.2556(5)	0.5207(7)	0.0090(5)
	P_5	0	0.2546(5)	0.5214(7)	0.0086(4)
	P_6	0	0.2553(5)	0.5200(7)	0.0081(4)
	P_7	0	0.2554(5)	0.5210(8)	0.0084(5)
	P_8	0	0.2551(6)	0.5199(8)	0.0077(5)
Al3	0.0001	0	0.44410(9)	0.5156(2)	0.0075(3)
4*a*	P_0^a	0	0.4444(8)	0.5151(5)	0.0072(4)
	P_1	0	0.4456(6)	0.5140(5)	0.0079(4)
	P_2	0	0.4457(5)	0.5134(6)	0.0082(4)
	P_3	0	0.4457(5)	0.5152(6)	0.0086(4)
	P_4	0	0.4453(5)	0.5188(7)	0.0090(5)
	P_5	0	0.4445(5)	0.5162(8)	0.0086(4)
	P_6	0	0.4443(5)	0.5170(8)	0.0081(4)
	P_7	0	0.4458(6)	0.5189(8)	0.0084(5)
	P_8	0	0.4465(6)	0.5202(9)	0.0077(5)
Al4	0.0001	0	0.29682(9)	0.1677(2)	0.0084(4)
4*a*	P_0^a	0	0.2966(7)	0.1676(5)	0.0072(4)
	P_1	0	0.2966(6)	0.1675(5)	0.0079(4)
	P_2	0	0.2954(5)	0.1667(6)	0.0082(4)
	P_3	0	0.2980(5)	0.1677(6)	0.0086(4)
	P_4	0	0.2965(5)	0.1677(6)	0.0090(5)
	P_5	0	0.2969(5)	0.1667(7)	0.0086(4)
	P_6	0	0.2973(5)	0.1658(7)	0.0081(4)
	P_7	0	0.2976(6)	0.1658(8)	0.0084(5)
	P_8	0	0.2979(7)	0.1677(8)	0.0077(5)
B	0.0001	0	0.0164(4)	0.0542(7)	0.0112(14)
4*a*	P_0^a	0	0.0201(17)	0.0549(13)	0.004(3)
	P_1	0	0.0176(15)	0.0542(13)	0.0079(4)
	P_2	0	0.0193(14)	0.0515(16)	0.0082(4)
	P_3	0	0.0209(14)	0.0482(17)	0.0086(4)
	P_4	0	0.0166(15)	0.0513(18)	0.0090(5)
	P_5	0	0.0177(15)	0.0555(19)	0.0086(4)
	P_6	0	0.0176(15)	0.0529(19)	0.0081(4)
	P_7	0	0.0186(17)	0.052(2)	0.0084(5)
	P_8	0	0.0173(17)	0.048(2)	0.0077(5)

Table 2 continued

Sites	P (GPa)	x	y	z	U_{iso}, U_{eq}
O1	0.0001	0	0.3285(2)	0.7049(5)	0.0090(8)
4*a*	P_0^a	0	0.3289(16)	0.700(1)	0.0082(6)
	P_1	0	0.3266(12)	0.7027(10)	0.0085(6)
	P_2	0	0.3262(10)	0.7016(11)	0.0068(7)
	P_3	0	0.3290(9)	0.6994(12)	0.0082(7)
	P_4	0	0.3265(10)	0.7008(14)	0.0083(8)
	P_5	0	0.3285(10)	0.7049(14)	0.0079(7)
	P_6	0	0.3308(10)	0.7014(14)	0.0067(7)
	P_7	0	0.3254(12)	0.7026(16)	0.0065(8)
	P_8	0	0.3238(13)	0.6990(16)	0.0036(8)
O2	0.0001	0.2558(4)	0.19016(15)	0.5345(3)	0.0073(6)
8*b*	P_0^a	0.2564(7)	0.1914(13)	0.5330(7)	0.0082(6)
	P_1	0.2566(8)	0.1882(10)	0.5345(7)	0.0085(6)
	P_2	0.2566(9)	0.1918(7)	0.5339(7)	0.0068(7)
	P_3	0.2567(9)	0.1908(7)	0.5335(8)	0.0082(7)
	P_4	0.2590(11)	0.1895(7)	0.5343(8)	0.0083(8)
	P_5	0.2566(10)	0.1905(7)	0.5308(9)	0.0079(7)
	P_6	0.2549(10)	0.1903(7)	0.5311(9)	0.0067(7)
	P_7	0.2582(12)	0.1891(8)	0.5337(9)	0.0065(8)
	P_8	0.2578(12)	0.1901(9)	0.5321(9)	0.0036(8)
O3	0.0001	0	0.4541(2)	0.9045(5)	0.0086(8)
4*a*	P_0^a	0	0.4535(15)	0.9073(10)	0.0082(6)
	P_1	0	0.4534(11)	0.9060(9)	0.0085(6)
	P_2	0	0.454(1)	0.9086(13)	0.0068(7)
	P_3	0	0.4554(8)	0.9062(14)	0.0082(7)
	P_4	0	0.4554(9)	0.9033(15)	0.0083(8)
	P_5	0	0.4536(9)	0.9100(16)	0.0079(7)
	P_6	0	0.4550(9)	0.9101(17)	0.0067(7)
	P_7	0	0.4561(11)	0.9008(17)	0.0065(8)
	P_8	0	0.4553(12)	0.9021(18)	0.0036(8)
O4	0.0001	0	0.0465(2)	0.4250(5)	0.0096(8)
4*a*	P_0^a	0	0.0434(14)	0.4261(11)	0.0082(6)
	P_1	0	0.0457(10)	0.4245(10)	0.0085(6)
	P_2	0	0.0477(8)	0.4260(13)	0.0068(7)
	P_3	0	0.0465(8)	0.4243(13)	0.0082(7)
	P_4	0	0.0468(8)	0.4194(16)	0.0083(8)
	P_5	0	0.0445(9)	0.4232(16)	0.0079(7)
	P_6	0	0.0463(8)	0.4246(16)	0.0067(7)
	P_7	0	0.0458(10)	0.4204(18)	0.0065(8)
	P_8	0	0.0480(11)	0.4180(19)	0.0036(8)
O5	0.0001	0	0.3522(2)	0.3716(5)	0.0090(8)
4*a*	P_0^a	0	0.348(2)	0.3721(9)	0.0082(6)
	P_1	0	0.3475(14)	0.3706(8)	0.0085(6)
	P_2	0	0.3503(11)	0.3738(10)	0.0068(7)
	P_3	0	0.3504(10)	0.3722(10)	0.0082(7)
	P_4	0	0.3516(11)	0.3692(11)	0.0083(8)
	P_5	0	0.3521(12)	0.3672(12)	0.0079(7)
	P_6	0	0.3534(12)	0.3712(12)	0.0067(7)
	P_7	0	0.3505(13)	0.3663(13)	0.0065(8)
	P_8	0	0.3530(16)	0.3698(13)	0.0036(8)
O6	0.0001	0	0.1911(2)	0.2671(5)	0.0076(8)

Table 2 continued

Sites	P (GPa)	x	y	z	U_{iso}, U_{eq}
4*a*	P_0^a	0	0.1908(17)	0.2687(10)	0.0082(6)
	P_1	0	0.1912(13)	0.2668(10)	0.0085(6)
	P_2	0	0.1933(10)	0.2667(11)	0.0068(7)
	P_3	0	0.1903(10)	0.2654(11)	0.0082(7)
	P_4	0	0.1898(11)	0.2626(13)	0.0083(8)
	P_5	0	0.1907(11)	0.2674(13)	0.0079(7)
	P_6	0	0.1904(11)	0.2658(13)	0.0067(7)
	P_7	0	0.1910(12)	0.2641(15)	0.0065(8)
	P_8	0	0.1933(13)	0.2628(16)	0.0036(8)
O7	0.0001	0.2110(5)	0.04838(16)	0.1183(3)	0.0097(6)
8*b*	P_0^a	0.2113(9)	0.0540(13)	0.1187(6)	0.0082(6)
	P_1	0.2105(8)	0.050(1)	0.1193(6)	0.0085(6)
	P_2	0.2106(8)	0.0491(8)	0.1201(7)	0.0068(7)
	P_3	0.2130(8)	0.0479(7)	0.1192(9)	0.0082(7)
	P_4	0.2112(9)	0.0472(7)	0.1216(8)	0.0083(8)
	P_5	0.2124(9)	0.0494(7)	0.1172(10)	0.0079(7)
	P_6	0.2124(10)	0.0489(7)	0.1188(10)	0.0067(7)
	P_7	0.2119(10)	0.0479(8)	0.1220(9)	0.0065(8)
	P_8	0.2117(10)	0.0478(10)	0.1223(9)	0.0036(8)

Anisotropic refinements have been performed only with the crystal in air (0.0001 GPa). U_{eq} is given for the anisotropic refinements, U_{iso} for the isotropic refinements

[a] With the crystal in the DAC without P medium

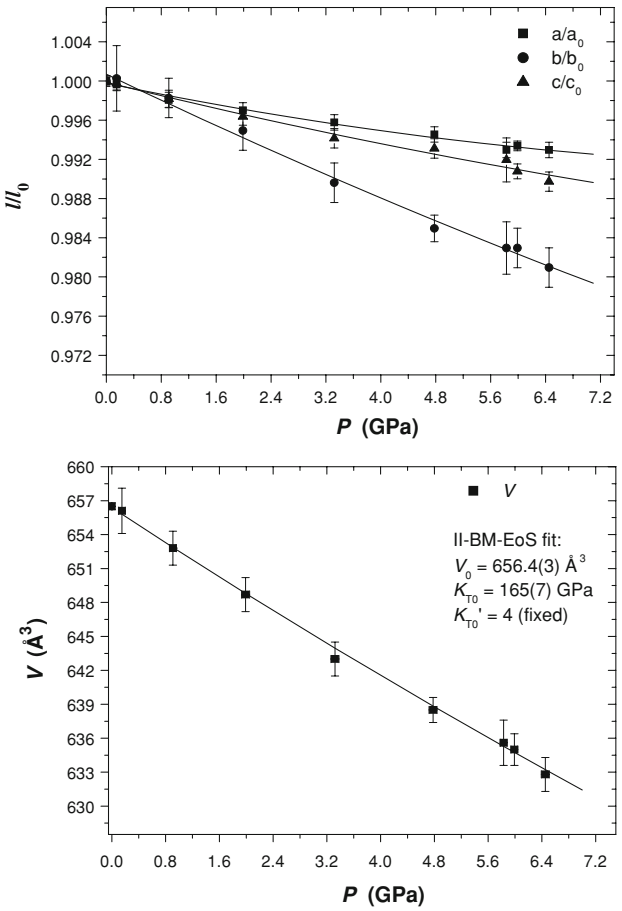

Fig. 2 Evolution of the unit-cell parameters of "Al_5BO_9" with pressure. For the unit-cell lengths, the *solid lines* represent polynomial regression curves through the data points. For the unit-cell volume, the second-order Birch-Murnaghan Equation-of-State fit is shown

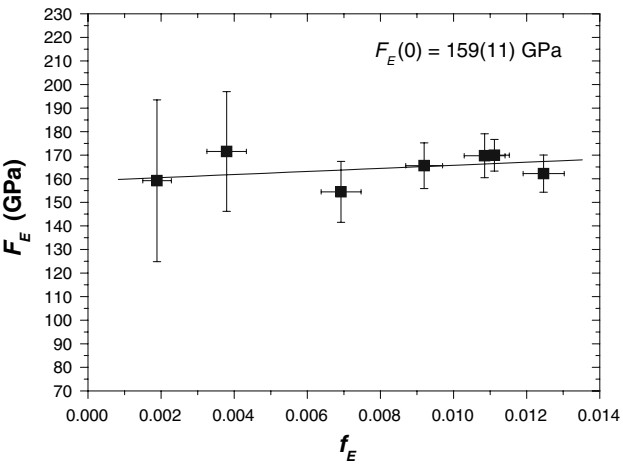

Fig. 3 Eulerian finite (f_E) strain versus normalized stress (F_E) plot. The weighted linear regression through the data points is shown

that the high-pressure strain energy in a solid can be expressed as a Taylor series in the Eulerian finite strain which is defined as

$$f_E = [(V_0/V)^{2/3} - 1]/2$$

where V_0 and V represent the unit-cell volume at ambient and HP conditions, respectively. Expansion in the Eulerian strain polynomial has the following form:

$$P(f_E) = 3K_{T0}f_E(1+2f_E)^{5/2}\{1 + 3/2(K'-4)f_E + 3/2[K_{T0}K'' + (K'-4)(K'-3) + 35/9]f_E^2 + \cdots\}$$

where K_{T0} represents the bulk modulus ($K_{T0} = -V_0(\partial P/\partial V)_{P=0} = 1/\beta_{V0}$, where β_{V0} is the volume compressibility coefficient at ambient conditions), K' and K'' represent its pressure derivatives ($K' = \partial K_{T0}/\partial P$; $K'' = \partial^2 K_{T0}/\partial P^2$). Fitting the P–V data with a truncated second-order (in energy) BM-EoS with the EOS-FIT5.2 program (Angel 2001), using the data weighted by the uncertainties in P and V, we obtain: $V_0 = 656.4(3)$ Å^3, $K_{T0} = 165(7)$ GPa ($\beta_{V0} = 0.0061(3)$ GPa^{-1}), and $K' = 4$ (fixed). A fitting with a third-order BM-EoS leads to a strong correlation between the refined parameters (especially K_{T0} and K'), with worse fitting statistic parameters.

The evolution of Eulerian finite strain versus normalized stress ($F_E = P/[3f_E(1+2f_E)^{5/2}]$) (Angel 2000) is shown in Fig. 3. The weighted linear regression through the data points leads to $F_E(0) = 159(11)$ GPa. The almost horizontal regression function confirms that the use of a

truncated II-BM-EoS is appropriate to describe the elastic behavior of "Al_5BO_9" within the P range investigated. The value of the normalized stress extrapolated at ambient conditions ($F_E(0)$) and the bulk modulus (K_{T0}) refined on the basis of the BM-EoS are in good agreement.

The axial compressibility coefficients [$\beta_j = 1/l_{0j}(\partial l_j/\partial P)$, where l_{0j} ($j = a, b, c$) is the length of the unit-cell edges under room conditions] were calculated by weighted polynomial regressions trough the data points, yielding to

$$a/a_0 = 1 - 0.0014(2)P + 6(3) \times 10^{-5}P^2 \quad (R^2 = 0.9906),$$
$$b/b_0 = 1 - 0.0034(4)P + 5(6) \times 10^{-5}P^2 \quad (R^2 = 0.9947),$$
$$c/c_0 = 1 - 0.0017(3)P + 4(5) \times 10^{-5}P^2 \quad (R^2 = 0.9855),$$

with $\beta_a = 1.4(2) \times 10^{-3}$ GPa^{-1}, $\beta_b = 3.4(4) \times 10^{-3}$ GPa^{-1}, $\beta_c = 1.7(3) \times 10^{-3}$ GPa^{-1} (β_a:β_b:β_c = 1:2.43:1.21).

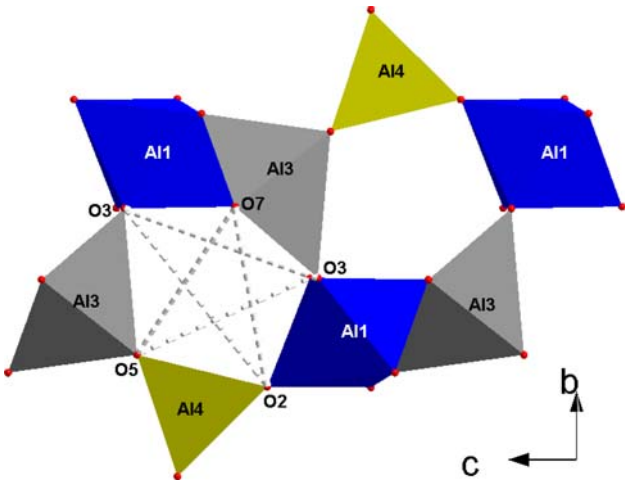

Fig. 4 Configuration of the voids represented by five-membered rings of polyhedra (i.e. Al1–Al3–Al4–Al1–Al3). The "diameters" of the voids (i.e. O7–O5, O7–O2, O3–O3, O3–O2 and O3–O5) are shown as *dashed lines*

Structural evolution with pressure

The single-crystal structural refinement of "Al_5BO_9" at room conditions confirms the structure model previously reported by Sokolova et al. (1978). Among the boroaluminosilicates, the topology of the "Al_5BO_9" structure is unique, although several structural homologies can be found with the mullite and mullite-type materials (e.g. sillimanite). In particular, the main building units are represented by edge-sharing octahedral chains linked by edge-sharing AlO_5 bipyramids alternating with AlO_4 tetrahedra, forming small cavities that host boron coordinated by three framework oxygens (BO_3 triangular units), as shown in Fig. 1. In the structural model of Sokolova et al. (1978) used in this study (i.e. space group $Cmc2_1$ with $a \sim 5.67$ Å, $b \sim 15.01$ Å, $c \sim 7.69$ Å), octahedral chains run parallel to [100]. Atomic positions, bond distances and angles refined in this study at room conditions agree with those previously reported (Table 2). Bond distances and angles show that octahedra, forming the [100] chains, and the tetrahedra are not regular (octahedron: $\langle Al1–O\rangle_{oct}$=1.903 Å and $\Delta(Al1–O)_{max} = 0.116$ Å; tetrahedron: $\langle Al4–O\rangle_{tet} = 1.753$ Å and $\Delta(Al4–O)_{max} = 0.041$ Å). The two bipyramidal units are strongly distorted (i.e. $\Delta(Al2–O)_{max} = 0.418$ Å and $\Delta(Al3–O)_{max} = 0.516$ Å). The BO_3 triangular unit is almost regular, with $B–O_{max} = 1.382(4)$ Å and $B–O_{min} = 1.372(6)$ Å (i.e. $\Delta(B–O)_{max} = 0.010$ Å).

The refinements at HP conditions show only minor change of the "Al_5BO_9" structure (Table 2; ESM Table 3). The variation of the polyhedral bond distances and angles is not larger than 2(σ) within the P range investigated. In other words, between 0.0001 and 6.5 GPa, polyhedra behave as rigid units. A corresponding behavior is also found for the BO_3 unit (ESM Table 3). Polyhedral distortions at 6.5 GPa are comparable to those observed at room conditions (at 6.45 GPa: $\Delta(Al1–O)_{max} = 0.12$ Å, $\Delta(Al2–O)_{max} = 0.46$ Å, $\Delta(Al3–O)_{max} = 0.56$ Å, $\Delta(Al4–O)_{max} = 0.04$ Å, and $\Delta(B–O)_{max} = 0.01$ Å). However, inter-polyhedral angles and distances vary significantly with pressure, which are interpreted as the main compressional mechanisms governing the unit-cell elastic anisotropy. In particular, if the structure is viewed down [100], voids with pentagonal shape, formed by five-membered rings of polyhedra (i.e. Al1–Al3–Al4–Al1–Al3; Fig. 4) occur. The decrease of the O7–O5, O7–O2 and O3–O2 distances between 0.0001 and 6.45 GPa (−5.2, −4.6 and −2.7%, respectively) is significantly larger than the O3–O3 and O3–O5 ones (−1.6 and −1.1%) (Figs. 4, 5). The P-induced compression along O7–O5 and O7–O2 contributes more to the shortening of the b-axis, whereas the P-induced decrease of O3–O3 and O3–O2 distances controls compression along the c-axis (Fig. 4). Shortening of the O7–O5, O7–O2, O3–O2, O3–O3 and O3–O5 distances is ascribable to polyhedral tilting, rather than an intra-polyhedral compression, as shown by the evolution of the O–O–O angles inscribed in the pentagonal distorted rings. In particular, the O2–O3–O7 angle decreases from 85.8(2)° to 82.5(2)° (i.e. Δ(O2–O3–O7) ~ 3.6°) and O7–O3–O5 from 88.2(4)° to 87.0(3)° (i.e. Δ(O7–O3–O5) ~ 1.2°), whereas the variation of O3–O5–O2, O5–O2–O3 and O3–O7–O3 are <1°. These P-induced mechanisms lead to a preferred compression along [010].

Discussion and conclusions

The present in situ high-pressure experiment shows that "Al_5BO_9" remains crystalline at least up to 7.4 GPa, and

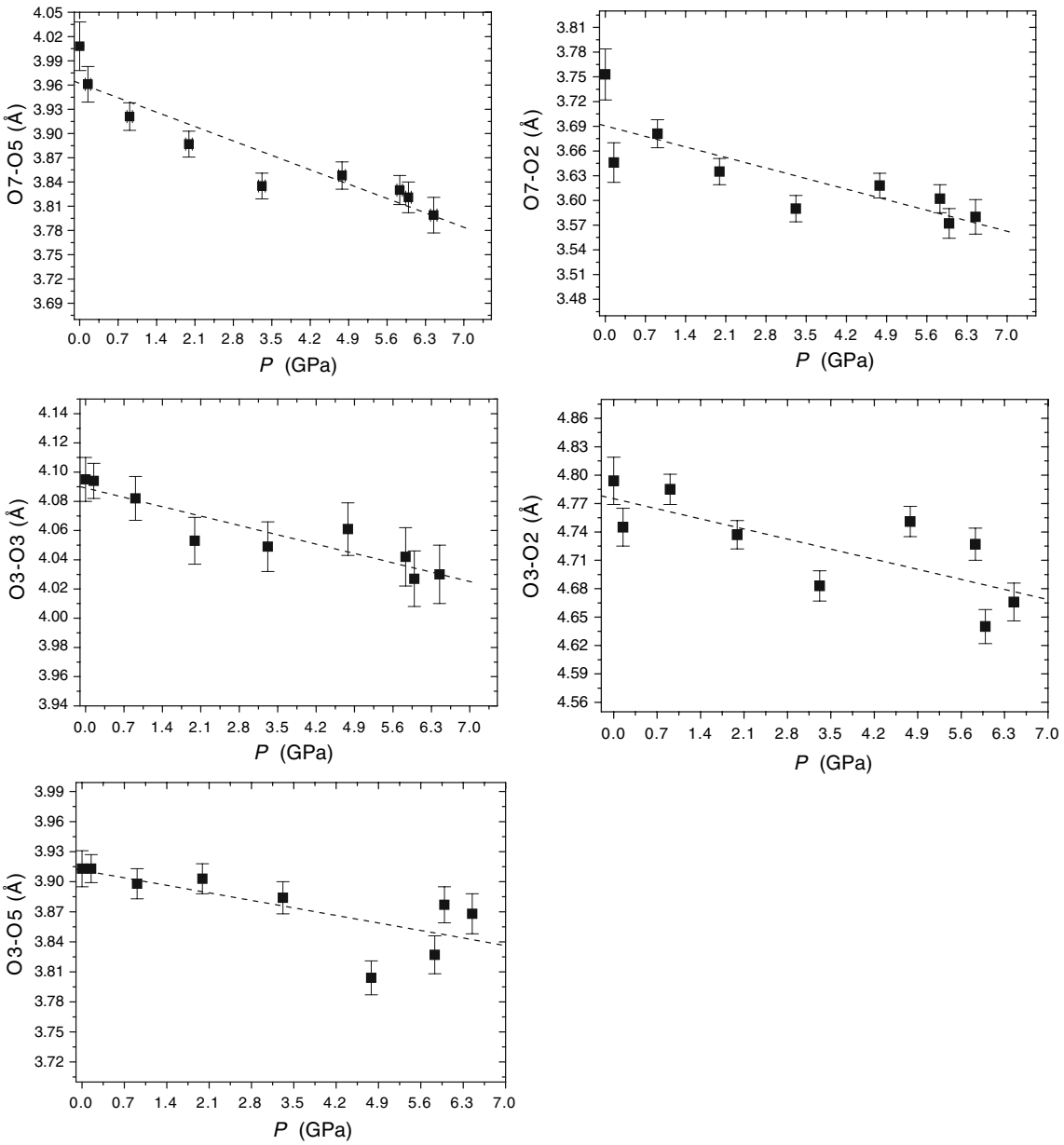

Fig. 5 Evolution of the O7–O5, O7–O2, O3–O3, O3–O2 and O3–O5 distances (i.e. "diameters" of the voids represented by the five-membered ring of polyhedra). *Dashed lines* represent the weighted linear regressions through the data points

any *P*-induced structural change is completely reversible. No phase transition or anomalous elastic behavior have been observed within the *P* range investigated, proving the high stability in elastic regime of this ceramic material at least up to 7.4 GPa.

The elastic analysis shows that "Al_5BO_9" is a stiff material. Its isothermal bulk modulus is similar to the one of mullite [adiabatic bulk modulus of 2:1 mullite: $K_S = 169.1$ GPa, Schreuer et al. (2006); 2:1 mullite: $K_S = 169.2$ GPa, Hildmann et al. (2001); 2.5:1 mullite: $K_S = 173.6.0$ GPa, Palko et al. (2002); 2.5:1 mullite: $K_S = 171.6$ GPa, Kriven et al. (1999); values recalculated by Schreuer et al. (2006) as average of Voigt and Reuss model] and sillimanite [$K_S = 171.4$ GPa, Vaughan and Weidner (1978); $K_{T0} = 171(1)$ GPa, Yang et al. (1997b), and $K_{T0} = 164(1)$ GPa, Burt et al. (2006)]. The elastic anisotropy of mullite-type materials observed in previous experiments is strikingly high [e.g. 2:1 mullite: $(s_{11} + s_{12} + s_{13}):(s_{21} + s_{22} + s_{23}):(s_{31} + s_{32} + s_{33}) = \beta_a:\beta_b:\beta_c = 1.40:1.86:1$, Hildmann et al. (2001); sillimanite: $\beta_a:\beta_b:\beta_c = 1.22:1.63:1$, based on single-crystal unit-cell parameters measured between 0.0001 and 5.3 GPa by Yang et al. (1997b), and $(3K_a)^{-1}:(3K_b)^{-1}:(3K_c)^{-1} = \beta_a:\beta_b:\beta_c = 1.82:2.63:1$, based on single-crystal unit-cell parameters measured between

0.0001 and 8.5 GPa by Burt et al. (2006)]. All the aforementioned studies showed that mullite-type materials are stiffer along the *c*-axis than along the *a*- or *b*-axis. For a comparative elastic analysis of the mullite-type materials extended to "Al_5BO_9", we have to consider an origin shift by $\mathbf{t} = (0, 0, 1/3)$ and a transformation matrix by $T = (\mathbf{b}, \mathbf{c}, \mathbf{a})$, according to Fischer and Schneider (2008), from $Cmc2_1$ setting used in this study and in Sokolova et al. (1978) to $Bb2_1m$ setting. In this light, there is a full agreement between the stiffer direction found in this study (i.e. [100]) and that found in mullite-type materials previously investigated (i.e. [001]). The higher compressibilities observed in this study within (100) can be ascribed to the presence of voids, which allow accommodating the effect of pressure by polyhedral tilting. Polyhedral tilting around the aforementioned five-membered rings (Al1–Al3–Al4–Al1–Al3) also explains the higher compressibility along [010] than along [001]. The stiffer crystallographic direction observed here might be controlled by the infinite chains of edge-sharing octahedra running along [100], which act as "pillars", making the structure less compressible along the *a*-axis than along the *b*- and *c*-axis. The reason is that along [100] compression can be accommodated only by deformation of the edge-sharing octahedra (and/or by compression of the Al–O bond lengths), as no polyhedral tilting can occur. In response to the applied pressure, any structure is expected to react first by tilting the polyhedra, then by distorting the polyhedra, and finally by decreasing the bond distances. This hierarchy is due to the fact that the first mechanism is energetically less costly than the other two (Gatta 2009).

Following the comparative analysis on the elastic behavior of mullite-type materials, we observed a similar elastic behavior between "Al_5BO_9" and mullite(s) or sillimanite along the direction of the octahedral chains, which is the less compressible direction, but a different behavior occurs in the plane perpendicular to the chains. Considering the aforementioned metrical relationship with other mullite-type materials, we expected that "Al_5BO_9" was more compressible along [001] than along [010]. However, we believe that this different elastic behavior on (100) is due to the different structural configuration on (100) in "Al_5BO_9" compared to other mullite-type materials. In particular, the presence of distorted bipyramids in "Al_5BO_9", which act as bridging units of the [100] octahedral chains and are not present in mullite or sillimanite, might explain the different elastic behavior on (100).

Acknowledgments GDG and NR thank the Italian CNR-Istituto per la Dinamica dei Processi Ambientali, Milano, for the financial support. MF and TA thank the Swiss National Science Foundation, Grant 200020-112198 "Crystal Chemistry of Minerals" for financial support. R.X. Fischer, an anonymous reviewer, and the Editor Milan Rieder are thanked for their efficient revision of the manuscript.

References

Angel RJ (2000) Equation of state. In: Hazen RM, Downs RT (eds) High-temperature and high-pressure crystal chemistry, vol 41: reviews in mineralogy and geochemistry. Mineralogical Society of America and Geochemical Society, Washington, pp 35–59

Angel RJ (2001) EOS-FIT V6.0. Computer program. Crystallography Laboratory, Department of Geological Sciences, Virginia Tech, Blacksburg

Angel RJ (2002) ABSORB V5.2. Computer program. Crystallography Laboratory, Department of Geological Sciences, Virginia Tech, Blacksburg

Angel RJ, McMullan RK, Prewitt CT (1991) Substructure and superstructure of mullite by neutron diffraction. Am Mineral 76:332–342

Angel RJ, Allan DR, Miletich R, Finger LW (1997) The use of quartz as an internal pressure standard in high-pressure crystallography. J Appl Crystallogr 30:461–466

Angel RJ, Bujak M, Zhao J, Gatta GD, Jacobsen SD (2007) Effective hydrostatic limits of pressure media for high-pressure crystallographic studies. J Appl Crystallogr 40:26–32

Baumann HN, Moore CH (1942) Electric furnace boroaluminate. J Am Ceram Soc 25:391–394

Birch F (1947) Finite elastic strain of cubic crystals. Phys Rev 71:809–824

Brace WF, Scholz CH, LaMori PN (1969) Isothermal compressibility of kyanite, andalusite and sillimanite from synthetic aggregates. J Geophys Res 74:2089–2098

Brunauer G, Frey F, Boysen H, Schneider H (2001) High temperature thermal expansion of mullite: an in situ neutron diffraction study up to 1600°C. J Eur Ceram Soc 21:2563–2567

Buick IS, Grew ES, Armbruster T, Medenbach O, Yates MG, Bebout GE, Clarke GL (2008) Boromullite, $Al_9BSi_2O_{19}$, a new mineral from granulite-facies metapelites, Mount Stafford, central Australia, a natural analogue of a synthetic "boron-mullite". Eur J Mineral 20:935–950

Burnham CW (1966) Computation of absorption corrections and the significance of end effect. Am Mineral 51:159–167

Burt JB, Ross NL, Angel RJ, Koch M (2006) Equations of state and structures of andalusite and sillimanite to 10 GPa. Am Mineral 91:319–326

Capponi JJ, Chenavas J, Joubert JC (1972) Nouveaux borates d'aluminium et de gallium obtenus par synthèse hydrothermale à haute pression. Bull Soc Franç Min Crist 95:412–417

Comodi P, Zanazzi PF, Poli S, Schmidt MW (1997) High-pressure behaviour of kyanite; compressibility and structural deformations. Am Mineral 82:452–459

Dietzel A, Scholze H (1955) Untersuchungen im system B_2O_3–Al_2O_3–SiO_2. Glastechn Ber 28:47–51

Fischer RX, Schneider H (2005) The mullite-type family of crystal structures. In: Schneider H, Komarneni S (eds) Mullite. Wiley, Weinheim, p 487

Fischer RX, Schneider H (2008) Crystal chemistry of borates and borosilicates with mullite-type structures: a review. Eur J Mineral 20:917–933

Fischer RX, Kahlenberg V, Voll D, MacKenzie KJD, Smith ME, Schnetger B, Brumsack HJ, Schneider H (2008) Crystal structure of synthetic $Al_4B_2O_9$: a member of the mullite family closely related to boralsilite. Am Mineral 93:918–927

Friedrich A, Kunz M, Winkler B, Le Bihan T (2004) High-pressure behaviour of sillimanite and kyanite: compressibility, decomposition and indication of a new high-pressure phase. Z Kristallogr 219:324–329

Garsche M, Tillmanns E, Almen H, Schneider H, Kupčik V (1991) Incorporation of chromium into aluminium borate $9Al_2O_3{\cdot}2B_2O_3(A_9B_2)$. Eur J Mineral 3:793–808

Gatta GD (2009) Extreme deformation mechanisms in open-framework silicates at high-pressure: evidence of anomalous intertetrahedral angles. Micropor Mesopor Mater. doi:10.1016/j.micromeso.2009.08.006

Gatta GD, Nestola F, Boffa Ballaran T (2006a) Elastic behaviour, phase transition and pressure induced structural evolution of analcime. Am Mineral 91:568–578

Gatta GD, Nestola F, Walter JM (2006b) On the thermo-elastic behaviour of kyanite: a neutron powder diffraction study up to 1200°C. Mineral Mag 70:309–317

Gatta GD, Rotiroti N, Fisch M, Kadiyski M, Armbruster T (2008) Stability at high-pressure, elastic behaviour and pressure-induced structural evolution of $CsAlSi_5O_{12}$, a potential nuclear waste disposal phase. Phys Chem Miner 35:521–533

Gielisse PJM, Foster WR (1962) The system Al_2O_3–B_2O_3. Nature 195:69–70

Grew ES, Graetsch HA, Pöter B, Yates MG, Buick I, Bernhardt HJ, Schreyer W, Werding G, Carson CJ, Clarke GL (2008) Boralsilite, $Al_{16}B_6Si_2O_{37}$, and "boronmullite": compositional variations and associated phases in experiment and nature. Am Mineral 93:283–299

Griesser KJ, Beran A, Voll D, Schneider H (2008) Boron incorporation into mullite. Mineral Petrol 92:309–320

Hildmann B, Ledbetter H, Kim S, Schneider H (2001) Structural control of elastic constants of mullite in comparison to sillimanite. J Am Ceram Soc 84:2409–2414

Ihara M, Imai K, Fukunaga J, Yoshida N (1980) Crystal structure of boroaluminate, $9Al_2O_3{\cdot}2B_2O_3$. Yogyo-Kyokai-Shi 88:77–84

Kim KH, Hummel FA (1962) Studies in lithium oxide systems: XII, Li_2O–B_2O_3–Al_2O_3. J Am Ceram Soc 45:487–489

Kriven WM, Palko JW, Sinogeikin S, Bass JD, Sayir A, Brunauer G, Boysen H, Frey F, Schneider J (1999) High temperature single crystal properties of mullite. J Eur Ceram Soc 19:2529–2541

Letort Y (1952) Contribution a l'étude de la synthèse de la mullite. Trans Int Ceram Congress 19–32

Li Y, Chang RPH (2006) Synthesis and characterization of aluminum borate ($Al_{18}B_4O_{33}$, $Al_4B_2O_9$) nanowires and nanotubes. Mater Chem Phys 97:23–30

Mazza D, Vallino M, Busca G (1992) Mullite-type structures in the systems Al_2O_3–Me_2O (Me = Na, K) and Al_2O_3–B_2O_3. J Am Ceram Soc 75:1929–1934

Miletich R, Allan DR, Kush WF (2000) High-pressure single-crystal techniques. In: Hazen RM, Downs RT (eds) High-temperature and high-pressure crystal chemistry, vol 41: reviews in mineralogy and geochemistry. Mineralogical Society of America and Geochemical Society, Washington, pp 445–519

Oxford Diffraction (2005) Oxford Diffraction Ltd., Xcalibur CCD system, CrysAlis Software system, Version 1.170

Palko JW, Sayir A, Sinogeikin SV, Kriven WM, Bass JD (2002) Complete elastic tensor for mullite ($2.5Al_2O_3{\cdot}SiO_2$) to high temperatures measured from textured fibers. J Am Ceram Soc 85:2005–2012

Peacor DR, Rouse RC, Grew ES (1999) Crystal structure of boralsilite and its relation to a family of boroaluminosilicates, sillimanite, and andalusite. Am Mineral 84:1152–1161

Peng LM, Li XK, Li H, Wang JH, Gong M (2006) Synthesis and microstructural characterization of aluminum borate whiskers. Ceram Int 32:365–368

Ralph RL, Finger LW, Hazen RM, Ghose S (1984) Compressibility and crystal structure of andalusite at high pressure. Am Mineral 69:513–519

Reynaud C (1977) Synthèse, analyse thermique et micrographie de nouveaux borates d'aluminium. Bull Soc Franç Min Crist 100:28–32

Rymon-Lipinski T, Hennicke HW, Lingenberg W (1985) Zersetzung von $9Al_2O_3{\cdot}2B_2O_3$ bei hohen Temperaturen. Keram Z 37:450–453

Saalfeld H, Guse W (1981) Structure refinement of 3:2-mullite ($3Al_2O_3{\cdot}2SiO_2$). N Jb Miner Mh 1981:145–150

Schneider H, Eberhard E (1990) Thermal expansion of mullite. J Am Ceram Soc 73:2073–2076

Schneider H, Komarneni S (2005) Mullite. Wiley, Weinheim, p 487

Schneider H, Schreuer J, Hildmann B (2008) Structure and properties of mullite—a review. J Eur Ceram Soc 28:329–344

Scholze H (1956) Über Aluminiumborate. Z Anorg Allg Ch 284:272–277

Schreuer J, Hildmann B, Schneider H (2006) Elastic properties of mullite single crystals up to 1400°C. J Am Ceram Soc 89:1624–1631

Sheldrick GM (1997) SHELX-97. Programs for crystal structure determination and refinement. University of Göttingen, Germany

Sokolova YeV, Azizov AV, Simonov MA, Leonyuk NI, Belov NV (1978) Crystal structure of synthetic ortho-3-borate $Al_5(BO_3)O_6$. Dok Akad Nauk SSSR 243:655–658

Tang CC, Elssfah EM, Zhang J, Chen DF (2006) Morphology- and composition-controlled synthesis of aluminium borate nanowires without catalysts. Nanotech 17:2362–2367

Tao X, Wang X, Li X (2007) Nanomechanical characterization of one-step combustion-synthesized $Al_4B_2O_9$ and $Al_{18}B_4O_{33}$ nanowires. Nano Letters 7:3172–3176

Vaughan MT, Weidner DJ (1978) The relationship of elasticity and crystal structure in andalusite and sillimanite. Phys Chem Miner 3:133–144

Wei S, Zhang J, Elsanousi A, Lin J, Shi F, Liu S, Ding X, Gao J, Qi S, Tang C (2007) From $Al_4B_2O_9$ nanorods to AlOOH (boehmite) hierarchical nanoarchitectures. Nanotech 18:255605 (6 p)

Werding G, Schreyer W (1984) Alkali-free tourmaline in the system MgO–Al_2O_3–B_2O_3–SiO_2–H_2O. Geochim Cosmochim Acta 48:1331–1344

Werding G, Schreyer W (1992) Synthesis and stability of werdingite, a new phase in the system MgO–Al_2O_3–B_2O_3–SiO_2 (MABS), and another new phase in the ABS-system. Eur J Mineral 4:193–207

Werding G, Schreyer W (1996) Experimental studies on borosilicates and selected borates. In: Grew ES, Anovitz LM (eds) Boron. Mineralogy, petrology, and geochemistry, vol 33: Reviews in mineralogy and geochemistry. Mineralogical Society of America and Geochemical Society, Washington, pp 117–163

Wilson AJC, Prince E (eds) (1999) International tables for X-ray crystallography, vol C: mathematical, physical and chemical tables, 2nd edn. Kluwer, Dordrecht

Winter JK, Ghose S (1979) Thermal expansion and high-temperature crystal chemistry of the Al_2SiO_5 polymorphs. Am Mineral 64:573–586

Yang H, Downs RT, Finger LW, Hazen RM, Prewitt CT (1997a) Compressibility and crystal structure of kyanite, Al_2SiO_5, at high pressure. Am Mineral 82:467–474

Yang H, Hazen RM, Finger LW, Prewitt CT, Downs RT (1997b) Compressibility and crystal structure of sillimanite, Al_2SiO_5, at high pressure. Phys Chem Miner 25:39–47

Zhang J, Lin J, Song HS, Elssfah EM, Liu SJ, Luo JJ, Ding XX, Tang C, Qi SR (2006) Bulk-quantity fast production of $Al_4B_2O_9$/$Al_{18}B_4O_{33}$ single-crystal nanorods by a novel technique. Mater Lett 60:3292–3295